

Near-Infrared Phosphorescent Switch of Diarylethene Phenylpyridinium Derivative and Cucurbit[8]uril for Cell Imaging

Conghui Wang, Yao-Hua Liu, and Yu Liu*

Near-infrared (NIR) pure organic room-temperature phosphorescence (RTP) materials have received growing research interest due to their wide application in the fields of high-resolution bioimaging and luminescent materials. In this work, the authors report a macrocycle-confined pure organic RTP supramolecular assembly, which is constructed by diarylethene phenylpyridinium derivative (DTE-TP) and cucurbit[8]uril (CB[8]). Compared with CB[6] and CB[7], the larger cavity of CB[8] induces molecular folding and enhances the intramolecular charge transfer interactions, which leads to the obtained assembly emitting efficient NIR phosphorescence at 700 nm. Due to the photochromism of the diarylethene core, the NIR phosphorescence is reversibly regulated by light irradiation at wavelengths of 365 and >600 nm. Furthermore, cell-based experiments show that this supramolecular assembly is located in the lysosomes and displays a NIR phosphorescence at 650–750 nm. In addition, by means of phosphorescence resonance energy transfer, the obtained assembly exhibits a red-shifted NIR emission at 817 nm. This supramolecular phosphorescent switch provides a convenient path for the modular design of water-soluble pure organic room-temperature NIR phosphorescent materials.

possess charge transfer characteristics tend to exhibit low excited state energies and red-shifted absorption.^[12,13] Macrocyclic host molecules could confine guest molecules to enhance the charge transfer interactions and induce efficient phosphorescence.^[14–16] Despite significant research efforts in the area of pure organic RTP, the development of a convenient strategy to construct a controlled NIR phosphorescent system remains a challenge.

In terms of practical applications, materials that exhibit controlled luminescence are of particular interest.^[17–20] For example, it has been reported that diarylethene and its derivatives can undergo efficient and reversible photochromism when irradiated with UV and visible light, ultimately allowing control of the luminescence of such compounds.^[21–25] The combination of NIR phosphorescence and photochromism in a single diarylethene molecule could therefore render such a system widely applicable in various

fields. However, to the best of our knowledge, photo-controlled pure organic NIR phosphorescence has yet to be reported in solution.

Thus, we herein report the preparation of a diarylethene phenylpyridinium derivative (DTE-TP) and its inclusion in the cavity of cucurbit[8]uril (CB[8]) through a unique folding configuration. The NIR phosphorescence of the resulting complex is evaluated at 700 nm, and the emission could be efficiently regulated through the diarylethene core (**Scheme 1**). Finally, to investigate the potential application of this system, a more red-shifted emission of 817 nm was obtained through phosphorescence resonance energy transfer. Besides, we examine its ability to exhibit photo-controlled NIR phosphorescence targeted bioimaging.

1. Introduction

Photoluminescent systems that exhibit near-infrared (NIR) phosphorescent emission at 700–1100 nm have attracted growing interest in recent years.^[1–3] Currently, most reported NIR phosphorescent systems are based on transition metal complexes, such as those of rhodium(I), ruthenium(II), platinum(II), and iridium(III).^[4–6] In such complexes, metal-to-ligand charge transfer (MLCT) can occur, which is beneficial to spin-orbit coupling, wherein modification of the chelating ligands could lead to a red-shift of the emission to achieve NIR phosphorescence.^[7,8] Compared with inorganic NIR phosphorescence, pure organic NIR room-temperature phosphorescence (RTP) is rare.^[9–11] Generally, organic molecules that

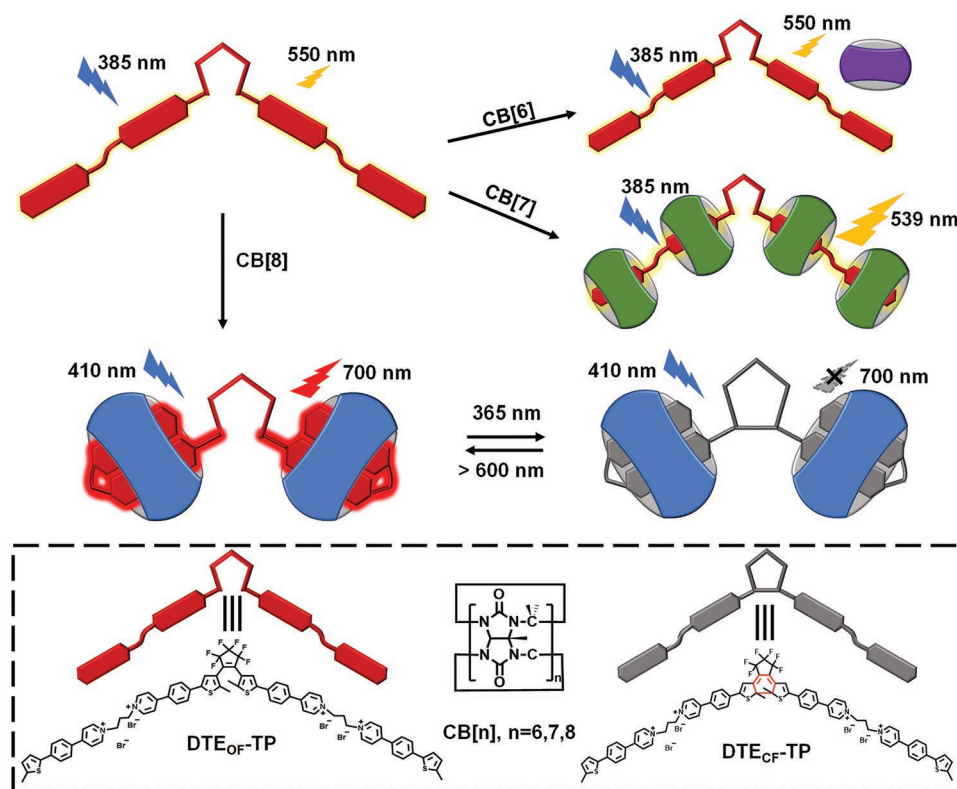
2. Results and Discussion

The synthetic routes toward DTE-TP and the reference compound (TP) are shown in the Supporting Information along with their characterization results (Schemes S1–S3 and Figures S1–S9, Supporting Information). As shown in **Figure 1a**, upon the addition of CB[8] to DTE-TP, the absorption spectrum showed a bathochromic shift from 383 to 411 nm, and the color of the

C. Wang, Y.-H. Liu, Y. Liu
College of Chemistry
State Key Laboratory of Elemento-Organic Chemistry
Nankai University
Tianjin 300071, P. R. China
E-mail: yuliu@nankai.edu.cn

 The ORCID identification number(s) for the author(s) of this article can be found under <https://doi.org/10.1002/sml.202201821>.

DOI: 10.1002/sml.202201821



Scheme 1. Schematic illustration and chemical structures of the photo-controlled NIR phosphorescence of DTE-TP/CB[8].

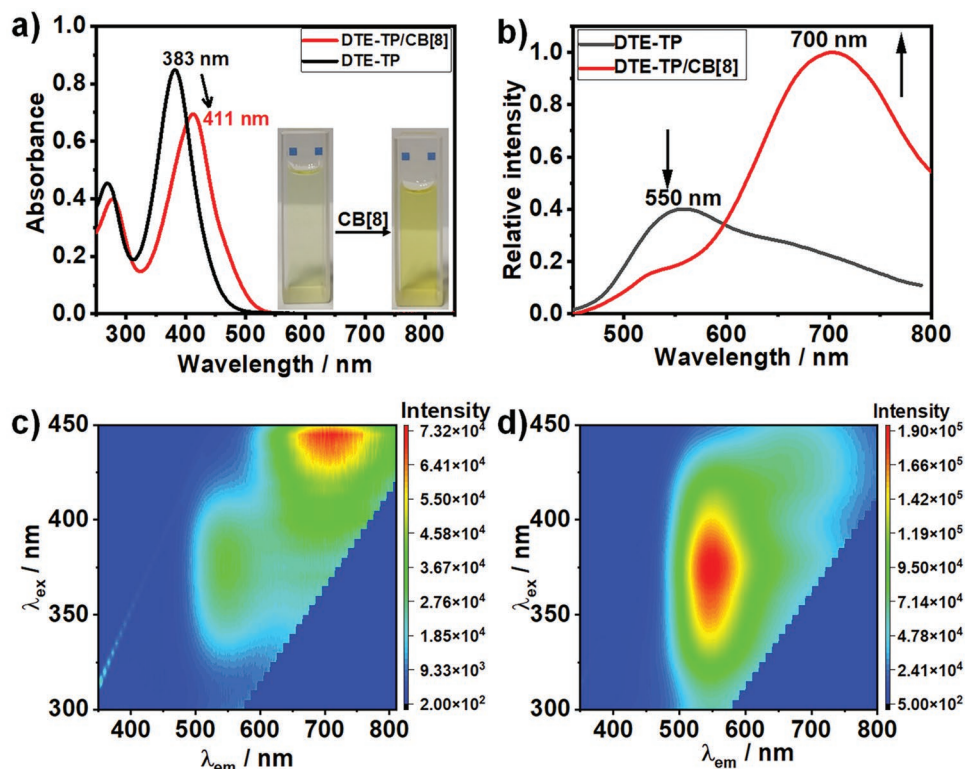


Figure 1. a) Changes in the absorption of DTE-TP (0.01 mM) following the addition of CB[8] (2 equiv.). b) Changes in the emission of DTE-TP (0.01 mM) following the addition of CB[8] (2 equiv.), where $\lambda_{\text{ex}} = 410$ nm. c) The emission map of DTE-TP/CB[8]. d) The emission map of DTE-TP.

solution changed from light yellow to deep yellow, implying the formation of a supramolecular assembly DTE-TP/CB[8]. Based on UV titrations (Figure S10, Supporting Information), the binding constant (K_s) was calculated to be $5.12 \times 10^{14} \text{ M}^{-2}$, which was in good agreement with the value obtained by isothermal titration calorimetry (Figure S11, Supporting Information). In addition, a Job's plot indicated a 1:2 binding stoichiometry for the DTE-TP/CB[8] complex (Figure S12, Supporting Information). Interestingly, upon the addition of greater quantities of CB[8] to the solution, the emission of DTE-TP at 550 nm gradually decreased, while a new peak at 700 nm gradually appeared and became more intense (Figure 1b). The emission map showed that the dominant emission band of DTE-TP was 550 nm under excitation between 330 and 410 nm, whereas DTE-TP/CB[8] exhibited two emission bands at 550 and 700 nm (Figure 1c,d). Upon increasing the excitation wavelength from 370 to 450 nm, the relative intensities of these two emission bands $I_{550 \text{ nm}}/I_{700 \text{ nm}}$ ($I_{550 \text{ nm}}$ and $I_{700 \text{ nm}}$ refer to the intensities at 550 and 700 nm, respectively), gradually decreased. In addition, when the fraction of dimethyl sulfoxide was increased, the emission band of DTE-TP/CB[8] at 700 nm disappeared, which confirmed that the NIR emission was due to the macrocyclic confinement of DTE-TP. More specifically, the increased quantity of organic solvent weakened the interactions between DTE-TP and CB[8], leading to disassembly of the complex (Figure S13, Supporting Information). As shown in Scheme 1, DTE-TP possesses two phenylpyridinium units linked by propyl groups, which allows molecular self-folding to take place upon binding with CB[8]. It was therefore anticipated that this new NIR emission peak at 700 nm originated from such molecular self-folding upon complexation with CB[8].

To verify the above hypothesis, the ^1H NMR spectra of DTE-TP and DTE-TP/CB[8] were recorded (Figure S14, Supporting Information), and it was found that the NMR signals of DTE-TP were shifted upfield upon the addition of CB[8]. However, it should be noted that it was difficult to assign the NMR signals due to the poor solubility of DTE-TP in deuterium oxide (<0.01 mM). Hence, the reference compound TP was also synthesized to investigate binding to CB[8]. Accordingly, the ^1H NMR peaks of TP were assigned by means of 2D ^1H - ^1H correlated spectroscopy (COSY) experiments (Figure S15, Supporting Information). During the assignment, it was found that the aromatic protons of phenylpyridinium ($\text{H}_{\text{d-g}}$) shifted upfield after the addition of CB[8], whereas the non-aromatic protons ($\text{H}_{\text{a,i}}$) shifted downfield, thereby implying that the phenylpyridinium moiety was inside the cavity of CB[8], whereas the alkyl protons were located outside the cavity (Figure 2a). In addition, the CB[8] portal protons (H_x and H_y) split into two sets of equivalent peaks upon formation of the TP/CB[8] complex, indicating that the symmetrical charge density environment of the CB[8] portal had been disrupted.^[26,27] Furthermore, 2D diffusion ordered spectroscopy (DOSY) experiments gave diffusion coefficients of 4.31×10^{-10} and $2.71 \times 10^{-10} \text{ m}^2 \text{ s}^{-1}$ for TP and TP/CB[8], respectively, excluding the possibility of forming supramolecular polymers (Figure S15, Supporting Information). These results suggest that TP and DTE-TP adopted the same folding configuration within the CB[8] cavity, and that supramolecular polymers did not form.^[28–31]

The complexation process was also examined using CB[7] and CB[6] for comparison. Upon the addition of CB[7], the $\text{H}_{\text{f,g}}$ protons shifted upfield, whereas the $\text{H}_{\text{a,i}}$ protons shifted downfield, implying that CB[7] could also accommodate the phenylpyridinium moiety in its cavity, while the alkyl and thiophene segments were located outside the cavity (Figure S16a, Supporting Information). However, when CB[6] was employed, no proton shifts were observed, thereby suggesting that the macrocyclic ring was too small to accommodate the guest molecule (Figure S16b, Supporting Information).

The photophysical properties of an addition reference compound (Me) were then investigated to further confirm the photoluminescence mechanism (Figure 2b). Due to the lack of a propyl spacer in this reference compound, it was unable to form a folded configuration within the cavity of CB[8]. In this case, upon the addition of CB[8] to a solution of the reference compound, the absorption shifted from 368 to 377 nm, and the Job's plot showed 2:1 binding stoichiometry (Figure S17, Supporting Information). In addition, the emission of Me exhibited a bathochromic shift from 530 to 542 nm, while the emission maps of Me and Me/CB[8] displayed a single emission peak (Figure S18, Supporting Information). These results therefore suggest that although CB[8] was able to enhance the intermolecular charge transfer interactions with Me, NIR emission was not successfully achieved. In contrast, the TP reference compound, which possesses two phenylpyridinium groups, can form 1:1 host-guest complex with CB[8] (Figure S19, Supporting Information). As a result, the peak corresponding to the maximum absorption of TP gradually shifted from 385 to 412 nm upon the continuous addition of CB[8], while its emission peak at 550 nm decreased in intensity and a new peak was generated at 750 nm; these observations are similar to those described above for DTE-TP/CB[8]. Furthermore, the emission maps of TP and TP/CB[8] show a single main emission peak at 550 nm; however, an emission peak was observed at 750 nm for TP/CB[8] at an excitation wavelength >400 nm, which was not observed for TP alone (Figure S20, Supporting Information). These results therefore suggest that CB[8] induced the self-folding of TP and enhanced the degree of intramolecular charge transfer interactions to produce NIR emission.

As mentioned above, CB[6] and CB[7] possess smaller cavities than CB[8]. As a result, in the case of CB[6] the lack of complexation was confirmed by the comparable absorption and emission spectra obtained in the presence of DTE-TP (Figure 2b). Furthermore, when CB[7] was added to solutions of TP and DTE-TP, no obvious bathochromic shifts were observed for the absorption peak, and the corresponding Job's plots showed 1:2 and 1:4 binding stoichiometries for TP/CB[7] and DTE-TP/CB[7], respectively (Figure S21, Supporting Information). We also observed that upon the addition of CB[7], the emission peaks of the guest molecules (i.e., TP and DTE-TP) at $\approx 550 \text{ nm}$ increased in intensity and displayed a blue shift, which was the opposite phenomenon to that observed for CB[8] addition (Figure S22, Supporting Information). In addition, no new peaks were observed in the NIR region when CB[7] was employed. These results therefore demonstrate that the head-to-head arrangement formed upon binding with CB[8] could generate an intramolecular excimer, ultimately resulting in a new NIR emission signal.

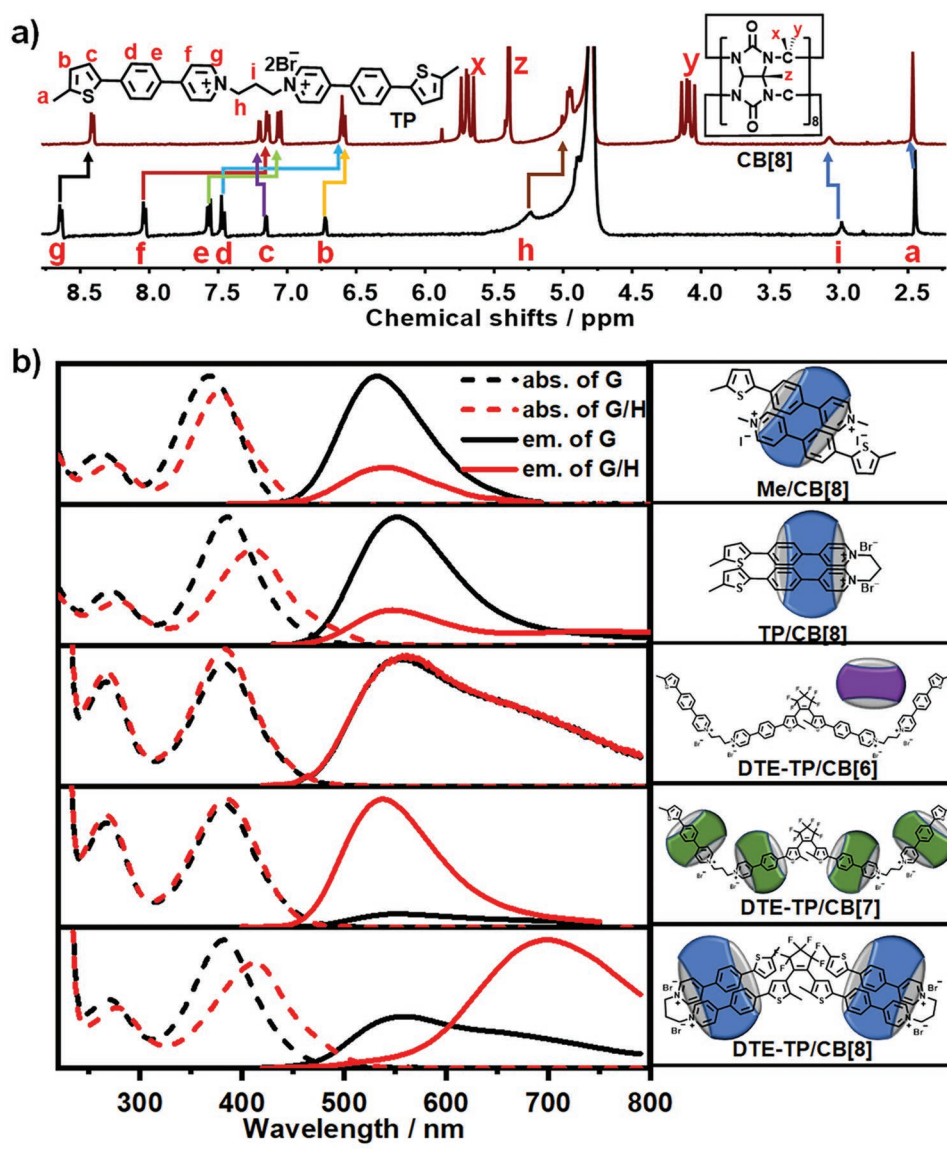


Figure 2. a) ¹H NMR spectra of TP and TP/CB[8] (400 MHz, D₂O). b) Left: absorption and photoluminescence spectra of the guest (G) and the host-guest (G/H) complex (G = Me, TP, or DTE-TP; H = CB[n], where n = 6, 7, or 8). Right: schematic illustration of the corresponding assemblies.

Interestingly, the emission intensities of the TP/CB[8] and DTE-TP/CB[8] complexes were found to increase with decreasing temperature, which is the typical characteristic of phosphorescence due to the low temperature could suppress the non-radiative transition (Figure 3a and Figure S23, Supporting Information). In addition, the gated emission overlapped well with the NIR emission, which also confirmed the phosphorescence property (Figure 3b and Figure S24, Supporting Information). It was also observed that the photoluminescence intensity was enhanced when N₂ was bubbled into the solution, and this was attributed to the fact that N₂ can protect the triplet excited state from quenching by species such as dissolved molecular O₂ (Figure 3c). Furthermore, the lifetimes of TP/CB[8] and DTE-TP/CB[8] were 1.58 and 0.93 μs, respectively (Figure S25, Supporting Information), while the quantum yields of TP/CB[8] and DTE-TP/CB[8]

were 5.41% and 1.12%, respectively (Table S1, Supporting Information).

Due to its photochromic character, we also considered the ability of DTE-TP to reversibly transfer between its two isomeric forms. As expected, upon irradiation with 365 nm UV light, the color of the DTE-TP solution changed from light yellow to light blue (Figure S26, Supporting Information), and a new absorption peak appeared at 645 nm, thereby indicating the formation of closed-form isomer (DTE_{CF}-TP). The conversion efficiency of DTE-TP was determined to be 90% based on the integral ratio changes in the ¹H NMR spectra (Figure S27, Supporting Information). Furthermore, when UV light was replaced by visible light (>600 nm), the color and absorption of the solution were restored to their initial states, implying the excellent reversibility (Figure S26, Supporting Information). As mentioned above, DTE-TP/CB[8] also showed a

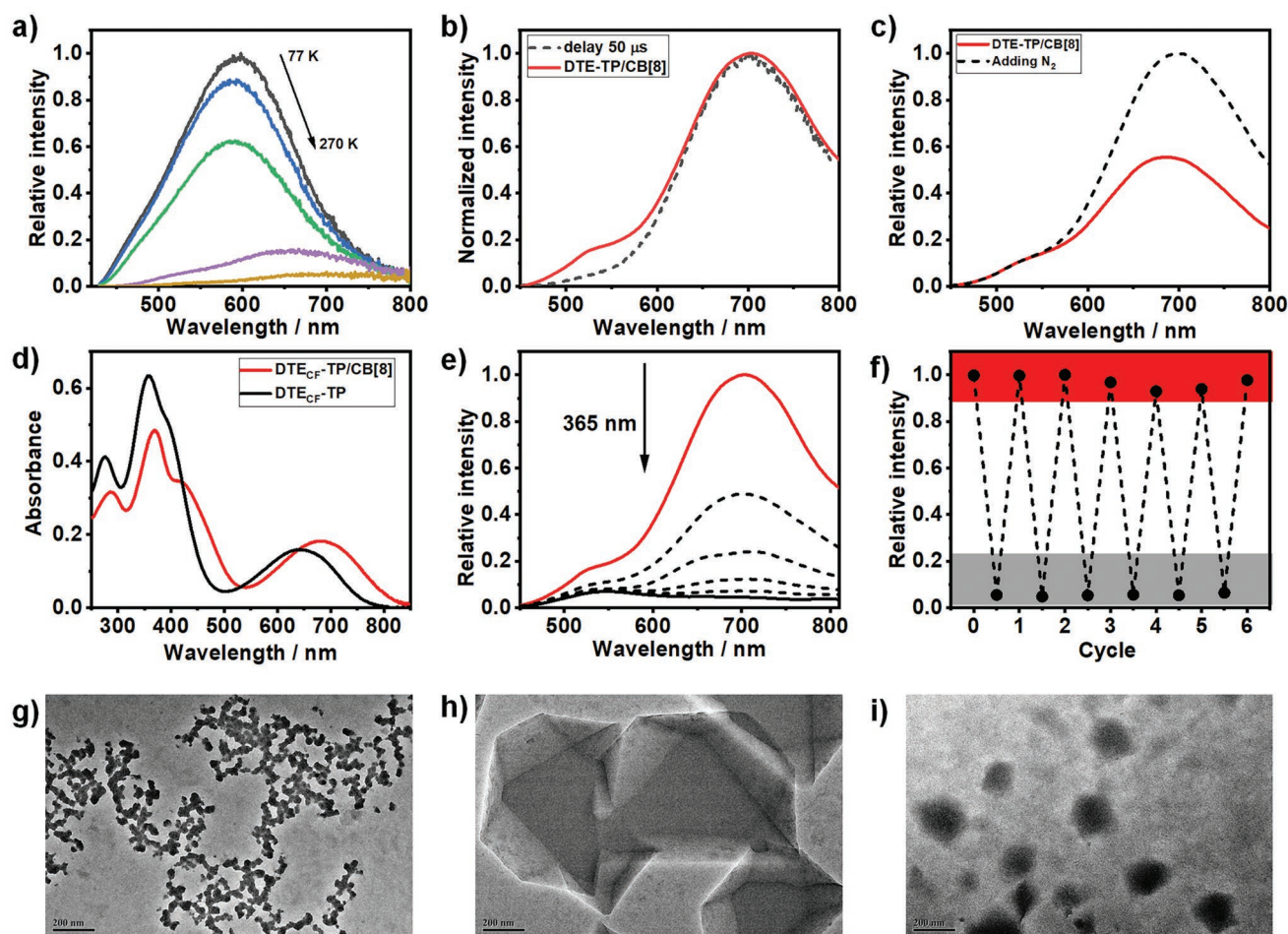


Figure 3. a) Photoluminescence spectra of DTE-TP/CB[8] at different temperatures. b) The phosphorescence and photoluminescence emission spectra of DTE-TP/CB[8]. c) The photoluminescence changes in DTE-TP/CB[8] during the bubbling of N₂ into the solution. d) UV-vis spectra of DTE_{CF}-TP and DTE_{CF}-TP/CB[8]. e) The photoluminescence changes in DTE_{OF}-TP/CB[8] upon 365 nm light irradiation. f) The emission intensity changes at 700 nm upon alternating 365 and >600 nm light irradiation. TEM images of g) DTE_{OF}-TP, h) DTE_{OF}-TP/CB[8], and i) DTE_{CF}-TP/CB[8].

satisfactory photochromic performance with a relatively rapid faster photochromic rate (Figure S28, Supporting Information). Compared with DTE_{CF}-TP, the absorption of DTE_{CF}-TP/CB[8] was red-shifted to 686 nm, suggesting that the assembly was stable despite the photochromism of DTE-TP (Figure 3d). The emission also exhibited the corresponding changes upon light irradiation, wherein the peak observed for DTE-TP/CB[8] at 700 nm gradually decreased in intensity upon irradiation with 365 nm UV light, eventually reaching a photostationary state (Figure 3e). The quenching efficiency was calculated to be 98% by comparing the emission intensities at 700 nm before and after UV light irradiation. Subsequently, the quenched emission was restored to its original state upon irradiation with >600 nm light (Figure S29, Supporting Information). Thus, as shown in Figure 3f, upon alternating between UV and visible light irradiation, this process could be repeated several times without any apparent photochemical damage, thereby implying that this system exhibits an excellent photoluminescent reversibility.

In terms of their particle morphologies, transmission electron microscopy (TEM) images of DTE-TP and TP revealed the presence of nanoparticles with diameters of ≈40 nm, while

CB[8] displayed a nanosheet topological morphology. In contrast, upon complexation, large polyhedra were generated (Figure 3g,h and Figure S30, Supporting Information). Upon irradiation with 365 nm UV light, the polyhedral morphology of DTE_{OF}-TP/CB[8] disappeared, and DTE_{CF}-TP formed nanoparticles with larger diameters (Figure 3i and Figure S30, Supporting Information). These photo-induced changes can be ascribed to the rigid plate structure of the closed-ring isomer.^[32]

NIR emission has great potential for application in disease diagnosis and clinical therapies owing to its deep tissue penetrability. Compared to the traditional rare-earth doped nanoparticles or quantum dots that have been examined for such purposes, DTE-TP/CB[8] was found to possess a large Stokes shift, and exhibited potential for use as a molecular switch for cell imaging. The stability of DTE-TP/CB[8] in water and its efficient photocontrolled NIR phosphorescence therefore encouraged us to further examine this supramolecular assembly as a potential NIR imaging agent. For this purpose, A549 cells (human lung cancer cell line) were incubated with DTE-TP/CB[8], and confocal microscopy observations were carried out. As shown in Figure 4a–c, following incubation, these cells emitted NIR

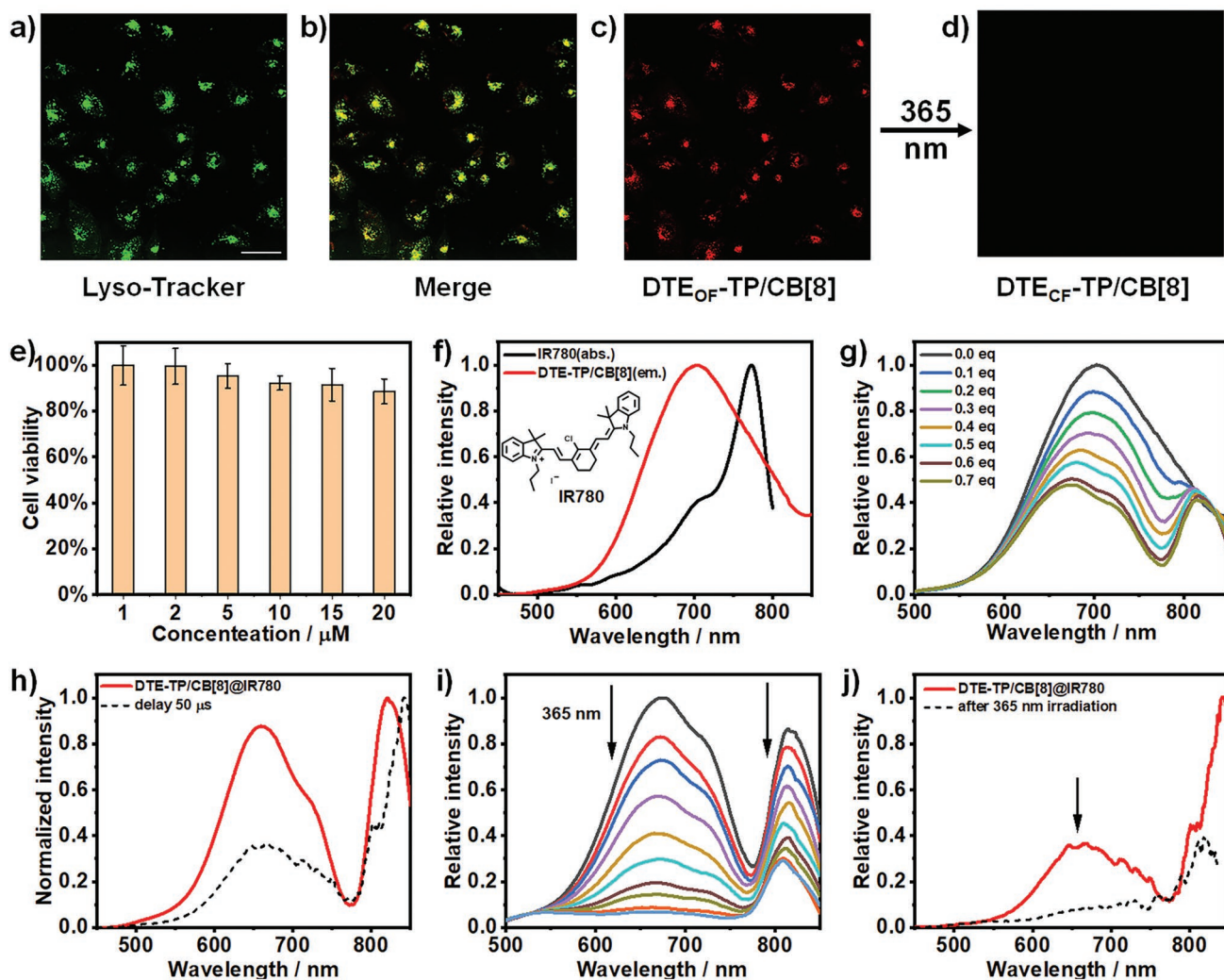


Figure 4. Laser confocal microscopy images of a) Lyso-Tracker Green, b) merged image, and c) DTE-TP/CB[8]. d) Laser confocal images of DTE-TP/CB[8] after 365 nm light irradiation. e) Cell viability values in the presence of 1–20 μM DTE-TP/CB[8]. f) Spectral overlap between the absorption of IR780 and the emission of DTE-TP/CB[8]. g) Changes in the photoluminescence of DTE-TP/CB[8] upon the addition of 0.0–0.7 equiv. IR780. h) Phosphorescence and photoluminescence emission of DTE-TP/CB[8]@IR780. i) Changes in the photoluminescence of DTE-TP/CB[8]@IR780 upon 365 nm light irradiation. j) Changes in the phosphorescence of DTE-TP/CB[8]@IR780 upon 365 nm light irradiation.

phosphorescence at 650–750 nm, and colocalization analysis confirmed that this NIR phosphorescence overlapped well with the lysosome marker Lyso-Tracker Green. Upon irradiation with 365 nm UV light, the DTE-TP/CB[8] was converted into its closed-form isomer, which led to NIR phosphorescence quenching, thereby indicating that efficient photo-controlled NIR phosphorescence lysosome-targeted cell imaging could be carried out using our system (Figure 4d). Importantly, the cellular viabilities were estimated to be >88% after 24 h in the presence of 0.2–20 μM DTE-TP/CB[8], which indicates that DTE-TP/CB[8] possessed low cytotoxicity (Figure 4e).

To further shift the emission of DTE-TP/CB[8] to longer NIR wavelengths, a suitable dye molecule, namely IR780 (a lipophilic cationic heptamethine dye), was added to the supramolecular assembly. As indicated in Figure 4f, the emission of DTE-TP/CB[8] overlapped well with the absorption of IR780, which allowed the subsequent energy transfer process to take place. As expected, the emission peak at 700 nm decreased in intensity

with the continuous addition of IR780 to the DTE-TP/CB[8] solution, while a new peak appeared at 817 nm (Figure 4g). The emission of IR780 was rather weak under the same excitation conditions, and the lifetime of DTE-TP/CB[8] decreased upon the addition of IR780, thereby suggesting that an efficient energy transfer process took place (Figures S31 and S32, Supporting Information). The gated emission spectrum (Figure 4h) confirmed that the peak at 817 nm corresponded to a long-lifetime photoluminescence, and it was found that the photochromism of DTE-TP under 365 nm UV light irradiation led to quenching of the NIR emission, confirming the occurrence of a photo-controlled NIR energy transfer process (Figure 4i,j).

3. Conclusion

We herein reported the construction of a macrocycle-confined pure organic room-temperature phosphorescent (RTP)

supramolecular assembly using a diarylethene phenylpyridinium derivative (DTE-TP) and cucurbit[8]uril (CB[8]). It was found that CB[8] induced the folding of DTE-TP to form a supramolecular assembly, and accelerated the photochromism of the diarylethene moiety. Furthermore, upon confinement of this guest molecule, the CB[8] host also enhanced the degree of intramolecular charge transfer interactions, resulting in near-infrared (NIR) RTP emission at 700 nm, which was subsequently red-shifted to 817 nm through phosphorescence resonance energy transfer. Owing to the excellent photochromic properties of the diarylethene core of the guest, it was possible to efficiently regulate the NIR phosphorescence emission by light irradiation at wavelengths of 365 and >600 nm. Finally, cell imaging experiments demonstrated the targeted and photocontrolled ability of this system to act as a supramolecular phosphorescence switch. Overall, the enhanced phosphorescence achieved using this macrocyclic confinement strategy provides a convenient approach for the materials with tunable functions.

Supporting Information

Supporting Information is available from the Wiley Online Library or from the author.

Acknowledgements

This work was financially supported by the National Natural Science Foundation of China (No. 22131008).

Conflict of Interest

The authors declare no conflict of interest.

Data Availability Statement

The data that support the findings of this study are available in the supplementary material of this article.

Keywords

cucurbituril, diarylethene, macrocycle, near-infrared, phosphorescence

Received: March 22, 2022

Revised: April 10, 2022

Published online:

- [1] G. N. A. De Guzman, M.-H. Fang, C.-H. Liang, Z. Bao, S.-F. Hu, R.-S. Liu, *J. Lumin.* **2020**, *219*, 116944.
- [2] H. Xiang, J. Cheng, X. Ma, X. Zhou, J. J. Chruma, *Chem. Soc. Rev.* **2013**, *42*, 6128.
- [3] Z. Liu, X. Dai, Y. Sun, Y. Liu, *Aggregate* **2020**, *1*, 31.
- [4] M. Schulze, A. Steffen, F. Wurthner, *Angew. Chem., Int. Ed.* **2015**, *54*, 1570.
- [5] S. Wang, K. Gu, Z. Guo, C. Yan, T. Yang, Z. Chen, H. Tian, W.-H. Zhu, *Adv. Mater.* **2019**, *31*, 1805735.
- [6] M. Cocchi, D. Virgili, V. Fattori, J. A. G. Williams, J. Kalinowski, *Appl. Phys. Lett.* **2007**, *90*, 023506.
- [7] M. Y. Leung, M. C. Tang, W. L. Cheung, S. L. Lai, M. Ng, M. Y. Chan, V. W.-W. Yam, *J. Am. Chem. Soc.* **2020**, *142*, 2448.
- [8] M. C. Tang, M. Y. Leung, S. L. Lai, M. Ng, M. Y. Chan, V. W.-W. Yam, *J. Am. Chem. Soc.* **2018**, *140*, 13115.
- [9] W. Zou, Y. Zhu, C. Gu, Y. Miao, S. Wang, B. Yu, Y. Shen, H. Cong, *J. Mater. Sci.* **2020**, *55*, 9918.
- [10] S. Sun, L. Ma, J. Wang, X. Ma, H. Tian, *Natl. Sci. Rev.* **2022**, *9*, nwab085.
- [11] T. Zhang, X. Ma, H. Tian, *Chem. Sci.* **2020**, *11*, 482.
- [12] X. F. Wang, H. Xiao, P. Z. Chen, Q. Z. Yang, B. Chen, C. H. Tung, Y. Z. Chen, L. Z. Wu, *J. Am. Chem. Soc.* **2019**, *141*, 5045.
- [13] S. Zhu, B. C. Yung, S. Chandra, G. Niu, A. L. Antaris, X. Chen, *Theranostics* **2018**, *8*, 4141.
- [14] D.-A. Xu, Q.-Y. Zhou, X. Dai, X.-K. Ma, Y.-M. Zhang, X. Xu, Y. Liu, *Chin. Chem. Lett.* **2021**, *33*, 851.
- [15] Z. Y. Zhang, Y. Chen, Y. Liu, *Angew. Chem., Int. Ed.* **2019**, *58*, 6028.
- [16] W. L. Zhou, Y. Chen, Q. Yu, H. Zhang, Z. X. Liu, X. Y. Dai, J. J. Li, Y. Liu, *Nat. Commun.* **2020**, *11*, 4655.
- [17] X. Jiang, M. Lin, J. Huang, M. Mo, H. Liu, Y. Jiang, X. Cai, W. Leung, C. Xu, *Front. Chem.* **2020**, *8*, 559159.
- [18] M. I. Khazi, W. Jeong, J. M. Kim, *Adv. Mater.* **2018**, *30*, 1705310.
- [19] X. Yan, F. Wang, B. Zheng, F. Huang, *Chem. Soc. Rev.* **2012**, *41*, 6042.
- [20] Z. Y. Li, Y. Y. Liu, Y. J. Li, W. Wang, Y. Song, J. Zhang, H. Tian, *Angew. Chem., Int. Ed.* **2021**, *60*, 5157.
- [21] T. Fukushima, K. Tamaki, A. Isobe, T. Hirose, N. Shimizu, H. Takagi, R. Haruki, *J. Am. Chem. Soc.* **2021**, *143*, 5845.
- [22] S. Z. Hassan, S. H. Yu, C. So, D. Moon, D. S. Chung, *Chem. Mater.* **2020**, *33*, 403.
- [23] O. Babii, S. Afonin, C. Diel, M. Huhn, J. Dommermuth, T. Schober, S. Koniev, A. Hrebonkin, A. Nesterov-Mueller, I. V. Komarov, A. S. Ulrich, *Angew. Chem., Int. Ed.* **2021**, *60*, 21789.
- [24] C. Wang, Y.-M. Zhang, H. Li, J. Zhang, Y. Zhou, G. Liu, X. Xu, Y. Liu, *Chin. Chem. Lett.* **2021** <https://doi.org/10.1016/j.ccl.2021.09.106>.
- [25] G. Liu, H. Zhang, X. Xu, Q. Zhou, X. Dai, L. Fan, P. Mao, Y. Liu, *Mater. Today* **2021**, *22*, 100628.
- [26] J. Wang, Z. Huang, X. Ma, H. Tian, *Angew. Chem., Int. Ed.* **2020**, *59*, 9928.
- [27] X. K. Ma, W. Zhang, Z. Liu, H. Zhang, B. Zhang, Y. Liu, *Adv. Mater.* **2021**, *33*, 2007476.
- [28] C. Wang, X. K. Ma, P. Guo, C. Jiang, Y.-H. Liu, G. Liu, X. Xu, Y. Liu, *Adv. Sci.* **2022**, *9*, 2103041.
- [29] Z. J. Zhang, H. Y. Zhang, L. Chen, Y. Liu, *J. Org. Chem.* **2011**, *76*, 8270.
- [30] S. H. Li, X. Xu, Y. Zhou, Q. Zhao, Y. Liu, *Org. Lett.* **2017**, *19*, 6650.
- [31] W. S. Jeon, A. Y. Ziganshina, J. W. Lee, Y. H. Ko, J.-K. Kang, C. Lee, K. Kim, *Angew. Chem., Int. Ed.* **2003**, *115*, 4231.
- [32] K. Higashiguchi, G. Taira, J.-i. Kitai, T. Hirose, K. Matsuda, *J. Am. Chem. Soc.* **2015**, *137*, 2722.